JGP Journal of General Physiology

COMMUNICATION

Reinterpretation of the substrate specificity of the voltage-sensing phosphatase during dimerization

Martin Kruse[1], Susy C. Kohout[2], and Bertil Hille[3]

Voltage-sensing phosphatases (VSPs) cleave both 3- and 5-phosphates from inositol phospholipids in response to membrane depolarization. When low concentrations of *Ciona intestinalis* VSP are expressed in *Xenopus laevis* oocytes, the 5-phosphatase reaction can be observed during large membrane depolarizations. When higher concentrations are expressed, the 5-phosphatase activity is observed with smaller depolarizations, and the 3-phosphatase activity is revealed with strong depolarization. Here we ask whether this apparent induction of 3-phosphatase activity is attributable to the dimerization that has been reported when VSP is expressed at higher concentrations. Using a simple kinetic model, we show that these enzymatic phenomena can be understood as an emergent property of a voltage-dependent enzyme with invariant substrate selectivity operating in the context of endogenous lipid-metabolizing enzymes present in oocytes. Thus, a switch of substrate specificity with dimerization need not be invoked to explain the appearance of 3-phosphatase activity at high VSP concentrations.

Introduction

In this Communication, we reinterpret some observations in a recent article from one of our laboratories (Rayaprolu et al., 2018). That article reported the lipid substrate selectivity of the voltage-sensing lipid phosphatase of *Ciona intestinalis* (Ci-VSP; Okamura et al., 2018). This enzyme cleaves phosphates from the polyphosphorylated six-membered inositol ring of phosphoinositide lipids, the eponymous headgroup of this class of phospholipids. Ci-VSP is activated by membrane depolarization through a voltage-sensing domain closely related to those of voltage-gated ion channels. Phosphoinositides may be phosphorylated on the 3, 4, and 5 positions of the inositol ring, and the selectivity question in this Communication concerns the relative balance of the 5- and 3-phosphatase activities for the Ci-VSP enzyme.

When Ci-VSP was first described, it was assumed to function as a lipid 3-phosphatase because of its sequence similarity to PTEN (phosphatase and tensin homologue deleted on chromosome 10), a well-characterized 3-phosphatase (Murata et al., 2005). Further studies showed that Ci-VSP activation in *Xenopus laevis* oocytes and HEK293 cells depleted phosphatidylinositol-4,5-bisphosphate ($PI(4,5)P_2$), suggesting that it functioned as both a 5- and a 3-phosphatase (Fig. 1 A; Murata and Okamura, 2007; Iwasaki et al., 2008; Halaszovich et al., 2009; Kurokawa et al., 2012; Liu et al., 2012). Substrate selectivity and preferences are observed in many enzyme reactions. For example, the PTEN enzyme removes the 3-phosphate from phosphatidylinositol-3,4,5-trisphosphate ($[PI(3,4,5)P_3$) more efficiently than from phosphatidylinositol-3,4-bisphosphate ($PI(3,4)P_2$) or phosphatidylinositol-3,5-bisphosphate ($PI(3,5)P_2$) (Campbell et al., 2003; Iwasaki et al., 2008). For Ci-VSP, physical state changes, including voltage and dimerization, have been suggested to switch the phosphatase between two catalytic states of different substrate preference (Grimm and Isacoff, 2016; Rayaprolu et al., 2018).

Early experiments with Ci-VSP considered its oligomerization state. Specifically, Ci-VSP molecules were found to express as monomers on the cell surface of *Xenopus* oocytes after injection of 1 ng cRNA and counting single photobleaching steps by TIRF microscopy (Kohout et al., 2008). In contrast, Rayaprolu et al. (2018) demonstrated by several criteria that the enzyme forms dimers when protein expression is increased. When 40 ng Ci-VSP cRNA was injected into *Xenopus* oocytes, differentially tagged Ci-VSP forms were able to pull each other down in a co-immunoprecipitation assay. In addition, Ci-VSP expressed using a CMV promoter in mammalian HEK293 cells revealed formation of dimers by a single-molecule pull-down assay and observation of more than one photobleaching step in TIRF microscopy.

The next experiment in the same article was a functional assay intended to ask whether dimerization differentially affected the 5- and 3-phosphatase activities in oocytes (Rayaprolu et al., 2018). It was suggested that the 3-phosphatase activity was augmented by dimerization. Here, we reconsider the interpreta-

[1]Department of Biology and Program in Neuroscience, Bates College, Lewiston, ME; [2]Department of Cell Biology and Neuroscience, Montana State University, Bozeman, MT; [3]Department of Physiology and Biophysics, University of Washington School of Medicine, Seattle, WA.

Correspondence to Bertil Hille: hille@uw.edu.

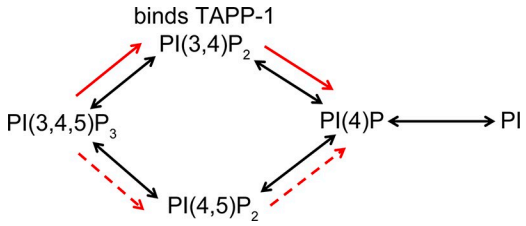

Figure 1. **Reaction scheme of the Keum et al. (2016) model.** Background endogenous kinase and phosphatase reactions in black arrows, and four phosphatase reactions catalyzed by VSP in red arrows. Fig. 2 concerns changes in $PI(3,4)P_2$ as measured by the fTAPP-1 indicator.

tion of those experiments by applying mathematical modeling of endogenous cellular enzymes in concert with the Ci-VSP activity.

Materials and methods

This Communication reprints one graph of experimental results from the article of Rayaprolu et al. (2018) and compares those data with original calculations from a kinetic model based on Keum et al. (2016). We summarize first the published experimental methods used to obtain the data under reanalysis, and then we describe the method of kinetic modeling. Both sets of methods have been described in detail recently in Rayaprolu et al. (2018) and Keum et al. (2016) from our laboratories, so they are given only in outline.

Oocyte experiments

Consider first the methods for the published experimental data that are the focus of our modeling and discussion. Ci-VSP in the pSD64TF vector from Y. Okamura (Osaka University, Osaka, Japan) and the TAPP-PH–based Förster resonance energy transfer (FRET) sensor (fTAPP) from E.Y. Isacoff (University of California, Berkeley, Berkeley, CA) were transcribed as complementary RNA (cRNA) using SP6 and T7 mMessage mMachine (Ambion) kits. cRNA concentrations ranging from 0.02 to 1.6 µg/µl encoding His-tagged Ci-VSP were mixed with fTAPP cRNA (0.4 µg/µl) and injected (50 nl) into surgically removed *X. laevis* oocytes. On the day of the experiments, cells were labeled with tetramethylrhodamine maleimide (TMRM; Rayaprolu et al., 2018) to recognize cells with good expression of Ci-VSP. Labeled oocytes were extensively washed in ND-96′ (96 mM NaCl, 2 mM KCl, 1.8 mM $CaCl_2$, 1 mM $MgCl_2$, and 10 mM HEPES, pH 7.6) and stored in ND-96′ containing 8 µM insulin to promote PI3 kinase activity and up-regulate $PI(3,4,5)P_3$ levels. Labeled, expressing oocytes were kept at 12–18°C until the end of the experiment.

FRET-based detection of $PI(3,4)P_2$ production and breakdown was performed using the pleckstrin homology (PH) domain from the tandem PH domain containing protein-1 (TAPP1) as previously described (Grimm and Isacoff, 2016; Rayaprolu et al., 2018). The FRET sensor (fTAPP) had an N-terminal CFP donor and a C-terminal YFP acceptor. Changes in $PI(3,4)P_2$ levels were indicated by changes of intramolecular FRET. Cells were viewed with an inverted microscope with a numerical aperture 0.7 fluorescence objective illuminated with an LED light source, and light intensity was measured with a photomultiplier tube. Appropriate excitation and emission filters allowed measurement of TMRM, CFP, and YFP emission.

The voltage protocol applied with a two-electrode voltage clamp consisted of a series of 2-s step pulses from –100 to 160 mV in irregular increments. Rest periods of 1 min between voltage steps allowed the depleted phosphoinositide concentrations to recover before the next voltage pulse. The resulting FRET change at the end of the pulse was plotted versus the voltage to generate the FRET-versus-voltage relationship. The fTAPP data are shown as ΔFRET/FRET with error bars indicating SEM.

Mathematical modeling

The new mathematical modeling closely followed a simulation described previously (Keum et al., 2016). Briefly, the Virtual Cell software environment (available at http://www.nrcam.uchc.edu; University of Connecticut Health Center) was used to develop a kinetic simulation (ordinary differential equations) of the changes of cellular phosphoinositide levels when the voltage-sensitive lipid phosphatase was stimulated in situ. The model combines kinetic steps of the endogenous phosphoinositide metabolism of the cell, the effects of exogenous Ci-VSP that we expressed in the cells, the properties of the lipid-binding probe fTAPP to measure the dynamic changes of $PI(3,4)P_2$, and the deduced voltage dependence and catalytic rates of Ci-VSP. We included five endogenous lipid phosphatase reactions, five endogenous lipid kinase reactions, and four VSP phosphatase activities acting on the phosphoinositide pools as diagrammed in Fig. 1. Some rate constants for enzymatic reactions were adjusted manually to fit experimental data. Rate constants for individual reactions either are the same as in our previous publication (Keum et al., 2016) or are listed in Table 1. The new published model is available in the Virtual Cell Public Database under mkruse: Kruse_Kohout_Hille_CiVSP (http://vcell.org/; University of Connecticut Health Center).

Results and discussion

Experimental data

The PH domain of TAPP-1 was expressed in oocytes as an indicator of $PI(3,4)P_2$ in the plasma membrane. TAPP-1-PH was sandwiched between two fluorescent proteins (called fTAPP), so the optical readout was a change in FRET between the chromophores—an increase of FRET when $PI(3,4)P_2$ rose and a decrease when it fell, as diagrammed in Fig. 1 and Fig. 2 A. Oocytes were pretreated with insulin to activate a lipid 3-kinase, raising the membrane concentration of the VSP phosphoinositide substrate, $PI(3,4,5)P_3$. The $PI(3,4,5)P_3$ can be converted to $PI(3,4)P_2$ by the 5-phosphatase activity of Ci-VSP, and, in turn, $PI(3,4)P_2$ can be converted to PI(4)P by the 3-phosphatase activity. The Ci-VSP phosphatase was activated in a graded manner by a series of progressively larger step depolarizations of the plasma membrane (Fig. 2 B). With injections of 1.0 or 2.5 ng Ci-VSP cRNA (light blue and dark blue symbols), all voltage steps >0 mV increased the FRET, suggesting a net 5-phosphatase activity. In contrast, with injections of high amounts, 40 or 80 ng (gray and black symbols), even small depolarizations gave FRET increases, and larger depolarizations gave FRET decreases. This pattern had suggested an initial 5-phosphatase activity followed by a 3-phosphatase

Table 1. **Rate constants and parameters for the model**

Parameter	Value	Rationale for parameter
Free PI(4,5)P_2 (density)	5,000 μm^{-2}	Xu et al., 2003
Bound PI(4,5)P_2 (density)	10,000 μm^{-2}	To make total 15,000 μm^{-2}
PI(4)P (density)	4,000 μm^{-2}	Xu et al., 2003
PI (density)(held constant)	140,000 μm^{-2}	Xu et al., 2003
PI(3,4,5)P_3 (density)	1,338 μm^{-2}	FRET response PH-Btk
PI(3,4)P_2 (density)	1,200 μm^{-2}	Steady state of basal *PLC* and *DAGase*
k_VSP (5Pase on PI(4,5)P_2)	8.0 s^{-1}	Based on PH-PLCδ1 FRET
k_VSP (5Pase on PI(3,4,5)P_3)	2.0 s^{-1}	Based on PH-Btk and PH-TAPP1 FRET
k_VSP (3Pase on PI(3,4)P_2)	0.15 s^{-1}	Based on PH-TAPP1 and P4M FRET
k_VSP (3Pase on PI(3,4,5)P_3)	44.0 s^{-1}	Based on PH-Btk and PH-PLCδ1 FRET
PH-TAPP1-PI(3,4)P_2	213 μm^{-2}	Based on FRET
PH-TAPP1 (concentration)	1 μM	Based on fluorescence intensity
K_D_TAPP-1	0.1 μM	Based on FRET and Dowler et al., 2000
V_0.5_Ci-VSP	57 mV/95 mV	Villalba-Galea et al., 2013, Fig. 2 C/revised here for Fig. 2 D
z_Ci-VSP	1.56/1.4	Villalba-Galea et al., 2013, Fig. 2 C/revised here for Fig. 2 D

The four VSP rate constants *k_VSP* would be the maximum (fully activated by voltage) values for the red arrows in Fig. 1, chosen to simulate experiments when 50 ng cRNA was injected into the oocyte. These rates were scaled in proportion for each actual injected amount of cRNA, and they were multiplied by a Boltzmann factor between 0 and 1 to give the rates a voltage dependence. Five endogenous lipid kinases and five endogenous lipid phosphatases (black arrows in Fig. 1) kept the same values as in our earlier publication (Keum et al., 2016). Concentrations of membrane molecules are expressed as density per unit area.

activity. Because this biphasic voltage-FRET behavior occurred only with injections of higher amounts of cRNA, the original article (Rayaprolu et al., 2018) reasoned that formation of phosphatase dimers would be favored and that the dimerization might bring on the 3-phosphatase activity of Ci-VSP, a substrate selectivity-switching hypothesis. We now consider an alternative interpretation.

Mathematical model

Two of us (M. Kruse and B. Hille) were coauthors on a recent paper (Keum et al., 2016) that described a chemical kinetic model for the zebrafish *Danio rerio* Dr-VSP enzyme operating in a living cell. That model was developed to explain biphasic FRET–voltage curves resembling the black and gray curves in Fig. 2 B but from experiments using Dr-VSP in a mammalian cell line. It considered all the metabolic steps in Fig. 1. The same model can be useful in discussing the experiments of Rayaprolu et al. (2018). We start by describing several key assumptions of the model. (a) The model recognized that in the context of a living cell, the depolarization-evoked phosphatase activities of VSP would become obvious only when they equaled or exceeded the corresponding cellular, voltage-independent endogenous phosphatase activities that operate in the background. Therefore, the kinetic model combines the phosphatase and kinase reactions of endogenous phosphoinositide metabolism (black arrows in Fig. 1) together with the four phosphatase reactions of exogenous VSP (red arrows in Fig. 1). (b) The voltage dependences of the four VSP reactions were assumed to be identical and to follow the same single Boltzmann curve modeled after that for the gates of a voltage-dependent ion channel. Thus, there would be no specificity changes with voltage, just a proportional increase in all rates. As usual, the Boltzmann curve was characterized by a midpoint voltage and an equivalent valence (a slope factor that governs the steepness of the voltage dependence) initially taken from sensing charge-movement measurements in the literature (Falkenburger et al., 2010). (c) The assumed maximum rate constants of the four VSP reactions were not identical, with the 5-phosphatase reactions being faster than the 3-phosphatase reactions at every voltage; that is, at all voltages, inositol 5-phosphates were assumed to be better substrates for this enzyme than inositol 3-phosphates are. Now consider the fTAPP FRET changes in Fig. 2 B, which report changes in PI(3,4)P_2. The biphasic black and gray FRET curves are explained qualitatively as follows. As depolarization progresses in steps from –100 mV, the larger 5-phosphatase of VSP will be the first VSP activity to exceed the rates of the endogenous metabolic machinery, so that the net rate of breakdown of PI(3,4,5)P_3 to PI(3,4)P_2 is accelerated and the FRET curve rises. However, with further depolarization, the activation of all the enzyme activities of VSP continues to be increased, and finally the VSP 3-phosphatase activity will also exceed the endogenous 3-phosphatases. Then the enlarged PI(3,4)P_2 pool will be further broken down to PI(4)P, and the FRET curve falls.

With this model in mind, we wondered whether it would be possible to explain the qualitative changes in Fig. 2 B as the cRNA concentration is increased without reference to specificity switching or to the reported monomer–dimer transition. Our reasoning was that with low Ci-VSP expression levels, the Ci-VSP enzyme velocities would be small, and the smaller 3-phosphatase

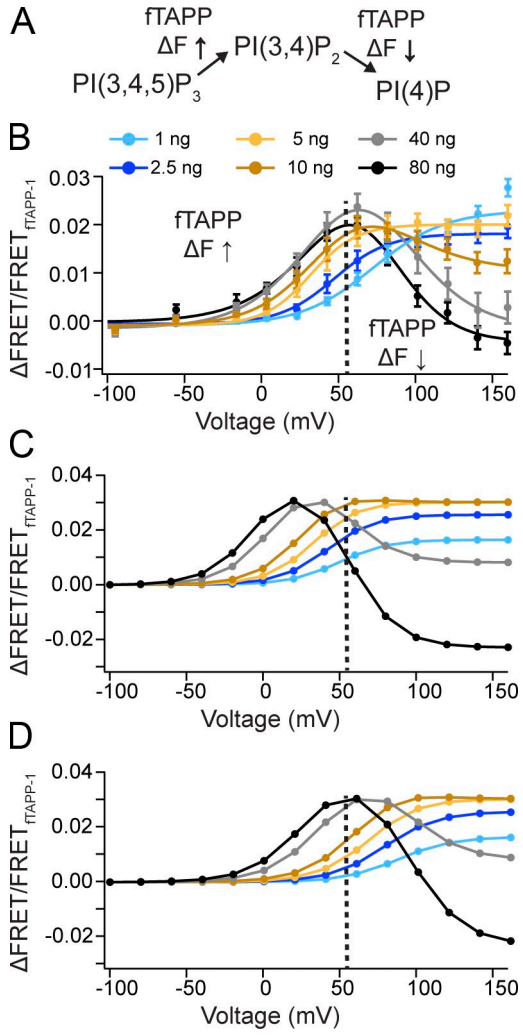

Figure 2. **Comparison of observed and modeled voltage dependence of fTAPP FRET with different expression levels of Ci-VSP in *Xenopus* oocytes. (A)** Reaction schematic of fTAPP assay where the fTAPP-1-PH FRET sensor shows an increase in FRET when $PI(3,4)P_2$ is produced and a decrease in FRET when $PI(3,4)P_2$ is depleted. **(B)** Normalized change of fTAPP-1 FRET ($\Delta FRET/FRET_{fTAPP-1}$) versus voltage relationships for six different cRNA injection amounts: 1 ng (light blue), 2.5 ng (blue), 5 ng (yellow), 10 ng (orange), 40 ng (gray), and 80 ng (black). A dashed vertical line is drawn at +56 mV. At high levels of Ci-VSP expression (40 and 80 ng cRNA injections), a FRET increase is observed with small depolarizations, changing to a FRET decrease with the largest depolarizations. At lower levels of Ci-VSP expression (1–5 ng cRNA injections), the FRET increase shifts to higher depolarizations and the FRET decrease is no longer detectable. Error bars are ±SEM, $n \geq 11$. Data are from Rayaprolu et al., 2018. **(C and D)** Simulations of curves in B using two models derived from Keum et al. (2016) as described in the text and Table 1. (C) Calculations using Boltzmann parameters taken from sensing-current measurements on Ci-VSP expressed in oocytes ($V_{0.5}$ = 57 mV, z = 1.56 electronic charges; Villalba-Galea et al., 2013). (D) Calculations with revised Boltzmann parameters: $V_{0.5}$ = 95 mV and z = 1.40 electronic charges. Simulations were done with Virtual Cell (http://www.nrcam.uchc.edu; University of Connecticut Health Center).

activities would never rise above the background level of endogenous metabolism. Therefore, only the 5-phosphatase component would become evident when activated enough by quite strong depolarizations, yielding a monophasic rising FRET–voltage curve. With higher Ci-VSP expression levels, sufficient 5-phosphatase activity would be activated by even modest depolarization, and larger depolarization would also elicit sufficient 3-phosphatase activity, yielding the biphasic curve. Fig. 2 C shows that a model with these assumptions captures the essential features of the original observations in Fig. 2 B. In particular, at the higher Ci-VSP protein levels (Fig. 2 C, gray and black traces), the model shows a robust rise and fall in FRET, indicating the breakdown of $PI(3,4,5)P_3$ to $PI(3,4)P_2$ and $PI(3,4)P_2$ to PI(4)P, similar to the experimental results in Fig. 2 B. And at lower concentrations of protein (Fig. 2 C, light blue, blue, and yellow traces), the model shows just a monotonic rise in FRET, again consistent with the results in *Xenopus* oocytes. Our initial model uses Boltzmann parameters measured with Ci-VSP in oocytes (Villalba-Galea et al., 2013; Table 1) and makes small adjustments of several rates and relative 5-phosphatase and 3-phosphatase selectivities for Ci-VSP instead of Dr-VSP. This calculation assumes that all four VSP enzyme rates increase in exact proportion with the amount of injected cRNA. Table 1 lists those rate constants and starting values that were changed from the original Keum et al. (2016) model parameters. The model assumes no effects from protein dimerization on enzymatic reactions. Nevertheless, physical characteristics, such as dimerization, may still impact VSP activity in other ways, including heterodimerization of homologues such as *X. laevis* VSP 1 and 2 or human VSP 1 and 2.

The simulations in Fig. 2 C capture key qualitative features of the experimental data in Fig. 2 B. Nevertheless, a couple of quantitative discrepancies suggest that the model might be improved. For example, focusing on the black (80 ng RNA) curve in the experimental data (Fig. 2 B), there is little activation of the 5-phosphatase activity at 0 mV, and the FRET response reporting $PI(3,4)P_2$ reaches a peak near +56 mV (dashed vertical line in Fig. 2 B). In contrast, in our initial simulation (Fig. 2 C), the 5-phosphatase activation makes a considerable contribution at 0 mV and the FRET rise reaches a peak near +15 mV. This means that activation of the enzyme by voltage in the model occurs at a lower depolarization than it should. The model can be improved by changing the Boltzmann parameters of activation from the values reported for "on" sensing current in oocytes, $V_{0.5}$ = 57 mV, z = 1.56 electronic charges (Villalba-Galea et al., 2013; measured with a phosphatase-dead mutant), to $V_{0.5}$ = 95 mV and z = 1.40 electronic charges (Table 1 and Fig. 2 D). The following paragraphs suggest how such a large midpoint shift might be rationalized.

We consider several factors. First, a small shift could be needed if the two-electrode voltage clamp used for FRET and the cut-open oocyte clamp used for sensing current in a different laboratory were not fully compensated for their different junction potentials, reference electrodes, and solutions. However, the 38-mV shift here seems much larger than expected for junction potentials.

Instead, we recognize that activation of the VSP enzyme is more complicated than we have represented, and indeed the details of enzyme coupling to voltage-sensor movement are still not tightly specified by the literature. Some complexities are described here. Voltage-dependent state changes of wild-type and mutated VSPs have been investigated both by the voltage dependence of sensing charge movement and by the voltage dependence of fluorescence from fluorescent enzyme derivatives. Both

types of experiments have identified two or more sequential steps induced by depolarization. All experiments with active enzyme are complicated by the unavoidable depletion of $PI(4,5)P_2$ that occurs quickly during depolarization. The first studies on voltage-sensor motions in phosphatase-inactive Ci-VSP identified a "relaxed" state that occurs after "activation," indicating that the voltage sensor passes among three conformations (Villalba-Galea et al., 2008, 2013). The charge movement was fitted by a single Boltzmann curve, but the midpoint of this curve moved dramatically with large changes of starting potential, and the overall data were fitted to a five-state model. Fluorescence from a G214C mutant reacted with TMRM dye showed two kinetic components in time, the second one developing within a few hundred milliseconds. In one laboratory, the fluorescence voltage curve for the active form of the G214C mutant has been described by a single Boltzmann curve with a midpoint at 56 mV (Rayaprolu et al., 2018). In another laboratory, using genetic replacement of residues near the phosphatase domain by a fluorescent unnatural amino acid ANAP, the fluorescence curves have been described as a sum of two Boltzmann curves for the active enzyme and as only one Boltzmann curve for an inactive mutant enzyme (Sakata et al., 2016; Kawanabe et al., 2018). The curve for active enzyme lay at more positive voltage than for inactive enzyme, and the curves were different when a different wavelength of emitted fluorescence was monitored. With active enzyme, shortening the interval between successive depolarizing pulses from 60 to 1.2 s, intended to promote accumulating depletion of $PI(4,5)P_2$, shifted L555-ANAP fluorescence curves in the positive direction (Sakata et al., 2016), and consistent with this, recruiting a lipid 5-phosphatase to the membrane with rapamycin, to catalyze depletion of $PI(4,5)P_2$, also shifted the curve for G214C-TMRM in the positive direction (Kohout et al., 2010). A new description of fluorescence–voltage behavior of active Ci-VSP from Kawanabe et al. (2018) reports two Boltzmann midpoints of 27 and 83 mV for the G214C-TMRM mutant and of 28 and 115 mV for the L555-ANAP mutant. As a tentative model, the latter paper speculated that small depolarizations induce a "partially activated state" of the voltage-sensing domain with "weak enzyme activity," whereas larger depolarization induces a fully activated voltage sensor and full enzyme activation. The higher measured second Boltzmann midpoints fall in the range of our improved model, and for the enzyme we might consider the three states of the Kawanabe model as a resting state with no enzyme activity, a preactivated state with no or very little enzyme activity, and a fully activated state with full activity. Our simple model, as we have used it here, still has only one voltage-dependent transition and thus a single Boltzmann curve leading to activity. It seems to correspond to the higher-voltage, second transitions. Thus, it is clear that the literature does not yet give unique instructions on how to model enzyme activation, so our choice of shifted Boltzmann parameters is not in conflict with established facts.

Another apparent discrepancy even in the improved model of Fig. 2 D is that at the highest voltages, the simulated black curve shows too much 3-phosphatase activity compared with experiment (Fig. 2 B). The FRET change becomes strongly negative near 150 mV. We suggest that this apparent hyperactivity may arise because 80 ng of RNA is quite a high amount for oocyte expression. We presume that at such high RNA concentrations, the assumed linear relation between RNA and expressed enzyme activity begins to deviate. A small sublinearity might reposition the 80-ng simulated curve somewhere between the gray (40 ng) and black (80 ng) curves on our present plot.

Conclusion

In summary, we argue that the native complement of endogenous enzymes present in living cells needs to be considered when evaluating exogenous enzymes expressed in them. We showed that this can be done by kinetic simulation. We added exogenous Ci-VSP activity to a previously published model that simulates cellular phosphoinositide metabolism in the context of native lipid kinases and phosphatases. We compared the model with recently published experimental data and found that the VSP activity observed using PH sensors can be explained by choosing fixed relative 5- and 3-phosphatase activities for VSP. The effects of both changing voltage and changing the level of enzyme expression can be described by one choice of enzymatic rate constants. It was not necessary to invoke a switching of enzyme substrate specificity with voltage or with dimerization. A second suggestion from the modeling is that activation of Ci-VSP by voltage occurs at voltages more positive than the midpoint of sensing charge measured with inactive VSP enzyme. We agree with the possibility of two steps during activation: the first involves a significant charge movement and reaches a preactivated state, and the second turns on the phosphatase activity. The calculations illustrate the value of kinetic simulation when dissecting enzyme rates in the complex environment of living cells with several active enzymes working on the same substrates.

Acknowledgments

We thank Vamseedhar Rayaprolu and Jason Castro for comments on the manuscript and William N. Zagotta for discussion.

This work was supported by National Institutes of Health (NIH), National Institute of General Medical Sciences grant R01GM111685 (to S.C. Kohout), NIH National Institute of Neurological Disorders and Stroke grant R37-NS08174-50 (to B. Hille), and the Wayne E. Crill Endowed Professorship (B. Hille). The Virtual Cell is supported by NIH National Institute of General Medical Sciences grant P41GM103313.

The authors declare no competing financial interests.

Author contributions: B. Hille conceived the paper. M. Kruse made the calculations. All authors participated in the writing.

Richard W. Aldrich served as editor.

Submitted: 26 September 2018
Accepted: 17 December 2018

References

Campbell, R.B., F. Liu, and A.H. Ross. 2003. Allosteric activation of PTEN phosphatase by phosphatidylinositol 4,5-bisphosphate. *J. Biol. Chem.* 278:33617–33620. https://doi.org/10.1074/jbc.C300296200

Dowler, S., R.A. Currie, D.G. Campbell, M. Deak, G. Kular, C.P. Downes, and D.R. Alessi. 2000. Identification of pleckstrin-homology-domain-containing proteins with novel phosphoinositide-binding specificities. *Biochem. J.* 351:19–31. https://doi.org/10.1042/bj3510019

Falkenburger, B.H., J.B. Jensen, and B. Hille. 2010. Kinetics of PIP_2 metabolism and KCNQ2/3 channel regulation studied with a voltage-sensitive phosphatase in living cells. *J. Gen. Physiol.* 135:99–114. https://doi.org/10.1085/jgp.200910345

Grimm, S.S., and E.Y. Isacoff. 2016. Allosteric substrate switching in a voltage-sensing lipid phosphatase. *Nat. Chem. Biol.* 12:261–267. https://doi.org/10.1038/nchembio.2022

Halaszovich, C.R., D.N. Schreiber, and D. Oliver. 2009. Ci-VSP is a depolarization-activated phosphatidylinositol-4,5-bisphosphate and phosphatidylinositol-3,4,5-trisphosphate 5′-phosphatase. *J. Biol. Chem.* 284:2106–2113. https://doi.org/10.1074/jbc.M803543200

Iwasaki, H., Y. Murata, Y. Kim, M.I. Hossain, C.A. Worby, J.E. Dixon, T. McCormack, T. Sasaki, and Y. Okamura. 2008. A voltage-sensing phosphatase, Ci-VSP, which shares sequence identity with PTEN, dephosphorylates phosphatidylinositol 4,5-bisphosphate. *Proc. Natl. Acad. Sci. USA.* 105:7970–7975. https://doi.org/10.1073/pnas.0803936105

Kawanabe, A., M. Hashimoto, M. Nishizawa, K. Nishizawa, H. Narita, T. Yonezawa, Y. Jinno, S. Sakata, A. Nakagawa, and Y. Okamura. 2018. The hydrophobic nature of a novel membrane interface regulates the enzyme activity of a voltage-sensing phosphatase. *eLife.* 7:e41653.

Keum, D., M. Kruse, D.I. Kim, B. Hille, and B.C. Suh. 2016. Phosphoinositide 5- and 3-phosphatase activities of a voltage-sensing phosphatase in living cells show identical voltage dependence. *Proc. Natl. Acad. Sci. USA.* 113:E3686–E3695. https://doi.org/10.1073/pnas.1606472113

Kohout, S.C., M.H. Ulbrich, S.C. Bell, and E.Y. Isacoff. 2008. Subunit organization and functional transitions in Ci-VSP. *Nat. Struct. Mol. Biol.* 15:106–108. https://doi.org/10.1038/nsmb1320

Kohout, S.C., S.C. Bell, L. Liu, Q. Xu, D.L. Minor Jr., and E.Y. Isacoff. 2010. Electrochemical coupling in the voltage-dependent phosphatase Ci-VSP. *Nat. Chem. Biol.* 6:369–375. https://doi.org/10.1038/nchembio.349

Kurokawa, T., S. Takasuga, S. Sakata, S. Yamaguchi, S. Horie, K.J. Homma, T. Sasaki, and Y. Okamura. 2012. 3′ Phosphatase activity toward phosphatidylinositol 3,4-bisphosphate [$PI(3,4)P_2$] by voltage-sensing phosphatase (VSP). *Proc. Natl. Acad. Sci. USA.* 109:10089–10094. https://doi.org/10.1073/pnas.1203799109

Liu, L., S.C. Kohout, Q. Xu, S. Müller, C.R. Kimberlin, E.Y. Isacoff, and D.L. Minor Jr. 2012. A glutamate switch controls voltage-sensitive phosphatase function. *Nat. Struct. Mol. Biol.* 19:633–641. https://doi.org/10.1038/nsmb.2289

Murata, Y., and Y. Okamura. 2007. Depolarization activates the phosphoinositide phosphatase Ci-VSP, as detected in Xenopus oocytes coexpressing sensors of PIP_2. *J. Physiol.* 583:875–889. https://doi.org/10.1113/jphysiol.2007.134775

Murata, Y., H. Iwasaki, M. Sasaki, K. Inaba, and Y. Okamura. 2005. Phosphoinositide phosphatase activity coupled to an intrinsic voltage sensor. *Nature.* 435:1239–1243. https://doi.org/10.1038/nature03650

Okamura, Y., A. Kawanabe, and T. Kawai. 2018. Voltage-Sensing Phosphatases: Biophysics, Physiology, and Molecular Engineering. *Physiol. Rev.* 98:2097–2131. https://doi.org/10.1152/physrev.00056.2017

Rayaprolu, V., P. Royal, K. Stengel, G. Sandoz, and S.C. Kohout. 2018. Dimerization of the voltage-sensing phosphatase controls its voltage-sensing and catalytic activity. *J. Gen. Physiol.* 150:683–696. https://doi.org/10.1085/jgp.201812064

Sakata, S., Y. Jinno, A. Kawanabe, and Y. Okamura. 2016. Voltage-dependent motion of the catalytic region of voltage-sensing phosphatase monitored by a fluorescent amino acid. *Proc. Natl. Acad. Sci. USA.* 113:7521–7526. https://doi.org/10.1073/pnas.1604218113

Villalba-Galea, C.A., W. Sandtner, D.M. Starace, and F. Bezanilla. 2008. S4-based voltage sensors have three major conformations. *Proc. Natl. Acad. Sci. USA.* 105:17600–17607. https://doi.org/10.1073/pnas.0807387105

Villalba-Galea, C.A., L. Frezza, W. Sandtner, and F. Bezanilla. 2013. Sensing charges of the *Ciona intestinalis* voltage-sensing phosphatase. *J. Gen. Physiol.* 142:543–555. https://doi.org/10.1085/jgp.201310993

Xu, C., J. Watras, and L.M. Loew. 2003. Kinetic analysis of receptor-activated phosphoinositide turnover. *J. Cell Biol.* 161:779–791. https://doi.org/10.1083/jcb.200301070